RESEARCH ARTICLE

International Journal of Climatology · RMetS

# Assessment of future wind speed and wind power changes over South Greenland using the Modèle Atmosphérique Régional regional climate model

Clara Lambin[1] | Xavier Fettweis[1] | Christoph Kittel[1,2] | Michaël Fonder[3] | Damien Ernst[3,4]

[1]Department of Geography, University of Liège, Liège, Belgium

[2]Université Grenoble Alpes/CNRS/IRD/G-INP, IGE, Grenoble, France

[3]Department of Electrical Engineering and Computer Science, University of Liège, Liège, Belgium

[4]LTCI, Telecom Paris, Institut Polytechnique de Paris, Paris, France

**Correspondence**
Clara Lambin, Department of Geography, University of Liège, Liège, Belgium.
Email: clara.lambin@uliege.be

## Abstract

Wind is an infinitely renewable energy source that is not evenly distributed in space and time. The interconnection of energy-demanding and energy-resourceful (yet remote) regions would help prevent energy scarcity in a world where fossil fuels are no longer used. Previous studies have shown that South Greenland and West Europe have complementary wind regimes. In particular, the southern tip of Greenland, Cape Farewell, has gained growing interest for wind farm development as it is one of the windiest places on Earth. In order to gain new insights about future wind speed variations over South Greenland, the Modèle Atmosphérique Régional (MAR), validated against in situ observations over the tundra where wind turbines are most likely to be installed, is used to build climate projections under the emission scenario SSP5-8.5 by downscaling an ensemble of CMIP6 Earth System Models (ESMs). It appeared that between 1981 and 2100, the wind speed is projected to decrease by $\sim-0.8$ m·s$^{-1}$ at 100 m a.g.l. over the tundra surrounding Cape Farewell. This decrease is particularly marked in winter while in summer, a wind speed acceleration is projected along the ice sheet margins. An analysis of two-dimensional wind speed changes at different vertical levels indicates that the winter decrease is likely due to a large-scale circulation change while in summer, the katabatic winds flowing down the ice sheet are expected to increase due to an enhanced temperature contrast between the ice sheet and the surroundings. As for the mean annual maximum wind power a turbine can yield, a decrease of $\sim-178.1$ W is projected at 100 m a.g.l. Again, the decrease is especially pronounced in winter. Considering the very high winter wind speeds occurring in South Greenland which can cut off wind turbines if too intense, the projected wind speed decrease might be beneficial for the establishment of wind farms near Cape Farewell.

# 1  |  INTRODUCTION

Global warming is one of the most important challenges of the 21st century and its mitigation requires, among others, replacing fossil fuels with renewable energy sources. Wind offers an advantage as it is infinitely renewable and non-polluting. Nonetheless, wind speeds required for efficient power harvesting are not equally distributed across the globe and over time (Radu *et al.*, 2019). Moreover, the distribution of the energy demand is not spatially uniform. As a result, some countries, especially the densely populated ones, do not have within their limits the sufficient renewable energy potential to satisfy their local demand (Berger *et al.*, 2021). Therefore, different concepts have emerged to address this issue. Firstly, the concept of a "global grid" proposes linking regions with complementary wind regimes in order to build a reliable worldwide power system (Chatzivasileiadis *et al.*, 2013). The main idea is to connect energy-demanding and energy-producing regions with long-distance power transmission lines that have been proven to be both technologically and economically feasible. By doing so, the intermittency issue of wind resources at a given place would be addressed by providing electricity from a high-yielding area in times of need. Because of the low local demand, exploiting the renewable energy potential of a remote resourceful area allows a large part of the generated electricity to be directly exported to high-demanding regions. Secondly, the concept of "remote renewable hubs" suggests that this electricity could be used to produce on-site carbon-neutral synthetic fuels that are then to be exported as well to high-demanding regions, as discussed in Berger *et al.* (2021).

In terms of wind power harvesting, the southern tip of Greenland, Cape Farewell (Figure 1), has been identified as a highly resourceful yet remote region (da Silva Soares, 2016; Jakobsen, 2016; Radu *et al.*, 2019). It is one of the windiest places on Earth due to the specific action of the Greenland Ice Sheet (GrIS) on the synoptic flow due to the presence of the Icelandic Low and the presence of cold katabatic winds flowing down the ice sheet (Moore *et al.*, 2015). Moreover, it appears that the temporal variability of the wind in this region is complementary with the European wind regime (Radu *et al.*, 2019). This means that in times of low wind power productivity, especially during summer, Europe could be supplied by Greenlandic wind farms to compensate for any energy production deficit with the implementation of this so-called global grid (Radu *et al.*, 2019).

In order to exploit the Greenlandic wind resources for electricity production, not only is a good knowledge of the current wind speed field necessary, but there is also a need to have an idea how it will change in the future. Because the Arctic is a region undergoing the strongest warming due to the Arctic amplification (Serreze and Francis, 2006), a long-term wind speed variability analysis would enable one to assess if wind speed is likely to be affected by climate change and therefore if there are any suitable prospects for wind farm development. To perform such an evaluation, using high-resolution climate models such as regional climate models (RCM) is relevant as they provide a continuous representation of the wind speed field in time and space, which is particularly useful in Greenland, an observation-scarce region. Moreover, RCMs can project wind changes at high spatial resolution under different emission scenarios by downscaling low-resolution Earth System Models (ESMs). Although the wind speed field over Cape Farewell has already been evaluated by a few studies using different
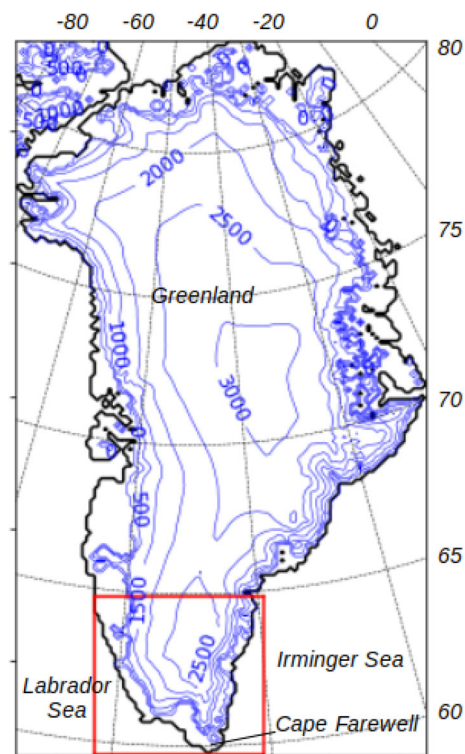


**FIGURE 1**    Greenland and surroundings modelled by MAR. The study area is represented by the red frame. The blue lines represent the ice sheet and its topography in meters [Colour figure can be viewed at wileyonlinelibrary.com]

RCMs (e.g., Bromwich *et al.*, 2001; Klein *et al.*, 2001; Ettema *et al.*, 2010b; Gorter *et al.*, 2014; Jakobsen, 2016), the long-term wind speed variability has not been comprehensively investigated at high spatial resolution. Gorter *et al.* (2014) used the Regional Atmospheric Climate Model (RACMO2) at a spatial resolution of 11 km to examine the change in the Weibull shape and scale parameters (which characterize the Weibull function of an asymmetrical distribution) of the wind speed distribution by the end of the 21st century, but only under the medium-range scenario of radiative forcing RCP4.5 (Radiative Concentration Pathway) from the Coupled Model Intercomparison Project phase 5 (CMIP5) (O'Neill *et al.*, 2016).

In this study, the RCM Modèle Atmosphérique Régional (MAR), version 3.12, has been chosen to evaluate the long-term wind speed variability over South Greenland under a high-end scenario of radiative forcing (SSP [Shared Socioeconomic Pathway] 5-8.5 from CMIP6). MAR has already been used multiple times over Greenland and has been proven to be well suited for the modelling of polar climates (e.g., Fettweis *et al.*, 2013; 2017; 2020). Although MAR wind speed outputs have been evaluated on a daily scale above the GrIS by Delhasse *et al.* (2020), they have not been evaluated over the ice-free area (tundra) of Greenland, which is the relevant area to investigate as the ice sheet is not appropriate for the installation of wind turbines due to ice dynamics.

The main objective of this paper is thus to investigate future wind speed and wind power changes by the year 2100 over Cape Farewell by analysing trends over the study area from projections built with MAR forced with an ensemble of CMIP6 ESMs. Prior to this analysis, an evaluation of hourly MAR wind speed outputs over the Greenlandic tundra will be carried out by comparing the model outputs with observation data, including a new set of data acquired during the Belgian KATABATA expedition (link to https://www.katabata-project.uliege.be/). Such an evaluation will provide good insights into whether or not the MAR-modelled wind speeds are reliable before performing the long-term wind speed analysis.

This paper is structured as such: Section 2 is a brief description of the wind regime in South Greenland. Section 3 includes a description of the study area (3.1), the observation data (3.2), the MAR model (3.3), simulations and forcing fields (3.4) used in this study. This sections also includes a summary of the MAR outputs evaluations (3.5) which is further detailed in the Supplement and a description of the methodology (3.6) used for the long term wind speed and power change analysis. Finally, results and discussion can respectively be found in Sections 4 and 5 while Section 6 gives the conclusions and perspectives.

## 2 | WIND REGIME IN SOUTH GREENLAND

The wind regime in South Greenland is driven by the katabatic winds originating from the ice sheet which can interact with the synoptic flow induced by the Icelandic Low. Katabatic winds occur on sloping terrains and result from a negative radiation balance at the surface which causes a downward sensible heat flux from the subjacent air layer to compensate for this radiation deficit (van den Broeke *et al.*, 1994). The latter is the result of the low heat absorption of the surface in short-wave radiation due to its high reflectivity and latitude associated with weak solar radiation and a relatively higher outgoing emission in long-wave radiation (Ettema *et al.*, 2010b; van As *et al.*, 2014). The downward sensible heat flux leads to the cooling of the near-surface air and generates an inversion layer (van den Broeke *et al.*, 1994). The lowering temperature of the air increases its density and the layer becomes negatively buoyant, creating a horizontal pressure gradient along the slope that drives the cooled near-surface air downslope combined with the action of the gravity force (van den Broeke *et al.*, 1994).

Over Greenland, the ice sheet cools the relatively warmer overlying air layer by radiative transfer and katabatic winds develop over a large part of it (Gorter *et al.*, 2014). Katabatic winds are characterized through their almost constant directional flow going down the ice sheet (considering the deviation by the Coriolis force). Their intensity, as well as the thickness of the katabatic layer, depends on the steepness and length of the slope, the temperature gradient of the inversion layer and the surface roughness. Over the GrIS, the weakest katabatic winds are found at the top of the ice sheet where the slopes are gentle while the strongest are found near its margins, especially along the southeastern coast, where the slopes are the steepest (Gorter *et al.*, 2014; Jakobsen, 2016).

Concerning the synoptic flow over Cape Farewell, it is mainly influenced by the presence of the Icelandic Low, located offshore between Greenland and Iceland. The Icelandic Low is a climatological low-pressure system, which is the net effect of all the meteorological lows passing over the Irminger Sea (Figure 1). The position of the Icelandic Low is close to the southeastern coast of Greenland during winter, while it shifts closer to the southern coast of Iceland during the summer. Its intensity is stronger in winter than in summer (Ettema *et al.*, 2010a). Because Greenland has a very high topography with its thick ice sheet that reaches 3,250 m above sea level (a.s.l.) (Jakobsen, 2016), the geostrophic flow associated with the low-pressure system is blocked and distorted by the orography. This leads to the creation of mesoscale low-level high wind speed events that are barrier winds and tip jets. Barrier winds occur along the

coast of Greenland while tip jets occur at the tip of Cape Farewell. The wind speed maxima of these phenomena are located above the ocean but their strong wind speeds can affect the tundra along which they occur (Moore and Renfrew, 2005). Over land, the katabatic winds can also add to the synoptic flow when flowing downwards in the same direction, leading to high and constant wind speeds, as it is the case over the ice-free area of Cape Farewell (Klein and Heinemann, 2002; Radu *et al.*, 2019).

## 3 | MATERIAL AND METHOD

### 3.1 | Study area

The area of interest in this study is the southern tip of Greenland, Cape Farewell (Figure 1). As explained previously, it is one of the windiest places on Earth as a consequence of a combination of katabatic winds from the GrIS with on-shore geostrophic winds and off-shore high-wind speed events such as tip jets and barrier winds. The selected area is located between 59.5°N and 64.5°N and between 40.0°W and 52.0°W.

### 3.2 | Observation data

The observation data used for the evaluation of MAR are in situ measurements obtained from multiple weather stations located in the study area. These stations are displayed in Figure 2 and are from three different databases: the Danish Meteorological Institute (DMI), the Program for Monitoring of the Greenland Ice Sheet (PROMICE) and the KATABATA project carried out by the University of Liège (Belgium). Details about the station locations are given in Table 1.

The KATABATA project was developed and conducted by two research units, SPHERES and MONTE-FIORE, from the University of Liège (ULiège) and aims at increasing the availability of in situ observations of katabatic winds at the southern tip of Greenland (https://www.katabata-project.uliege.be/). Therefore, three Finnish-made Vaisala automatic weather stations were installed in the ice-free area near Cape Farewell in September 2020. These stations have been established so as to be directly located in front of the prevailing winds, where previous MAR test simulations have identified wind speed maxima (Radu *et al.*, 2019). The stations measure temperature, humidity and horizontal wind speed with readings transmitted every 20 min by satellite connection. The wind speed is measured at 10 m above ground level (a.g.l.) and the temperature at 2 m a.g.l. The datasets from these stations range from September 2020 to the end of January 2021 for KAT 6640, the end of August 2021 for KAT 0460 and the end of February 2021 for KAT 0680. The time period differs from stations because some experienced a wind sensor failure during the winter of 2020/2021, but these
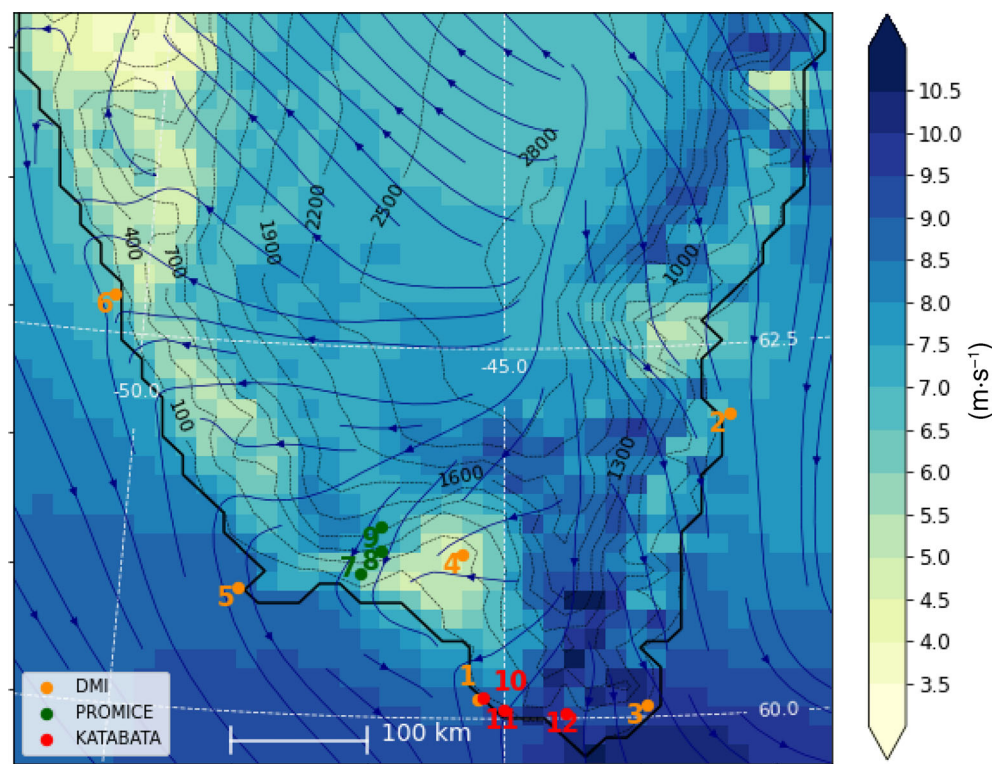


FIGURE 2 Mean wind speed (shaded colours), wind direction (streamlines) and station locations (coloured dots; see Table 1). The mean wind speed and direction were calculated on hourly data modelled by MAR from 2016 to 2018 forced with ERA-5 [Colour figure can be viewed at wileyonlinelibrary.com]

**TABLE 1** Detailed table of the station locations from Figure 2 as well as their available datasets time ranges

| Number | Station ID | Station name | Database | Lon. | Lat. | Elevation (m) | Time range |
|---|---|---|---|---|---|---|---|
| 1 | ANG | Angissoq | DMI | −45.15 | 59.99 | 4.38 | 2016–2018 |
| 2 | IKM | Ikeramiuarsuk | DMI | −42.07 | 61.94 | 39.59 | 2016–2018 |
| 3 | IKS | Ikerasassuaq | DMI | −43.17 | 60.06 | 88 | 2016–2017 |
| 4 | NAR | Narsarsuaq | DMI | −45.44 | 61.16 | 3.9 | 2018 |
| 5 | NUN | Nunarssuit | DMI | −48.45 | 60.76 | 32.6 | 2016–2018 |
| 6 | UKI | Ukiiviit | DMI | −50.41 | 62.58 | 22.23 | 2016–2018 |
| 7 | QAS_L | QAS_L | PROMICE | −46.85 | 61.03 | 280 | 2016–2018 |
| 8 | QAS_M | QAS_M | PROMICE | −46.83 | 61.10 | 630 | 2018 |
| 9 | QAS_U | QAS_U | PROMICE | −46.82 | 61.18 | 900 | 2016–2018 |
| 10 | KAT 6640 | AWS 6640 | KAT.-ULiège | −45.18 | 59.98 | 36 | Sep/2020–Jan/2021 |
| 11 | KAT 0460 | AWS 0460 | KAT.-ULiège | −45.07 | 60.16 | 76 | Sep/2020–Aug/2021 |
| 12 | KAT 0680 | AWS 0680 | KAT.-ULiège | −44.06 | 60.18 | 11 | Sep/2020–Feb/2021 |

*Note*: Time ranges of the available KATABATA-ULiège datasets do not cover the whole year so they are expressed in month/year. KAT.-ULiège stands for KATABATA-ULiège.

problems have been resolved thanks to a maintenance visit in July 2021. The KATABATA project has been implemented in the context of the "global grid" and the potential connections that could be made between West Europe and South Greenland in terms of renewable energy supply. Although the KATABATA stations have been installed specifically to assess the katabatic wind potential of Cape Farewell and to enable the evaluation of model performances to simulate these winds, their time series are relatively short and representative of a narrow area to evaluate our MAR climate model in depth. This is why, in addition to time series from the KATABATA project, PROMICE and DMI data have been used in the evaluation of MAR hourly wind speed outputs.

The PROMICE stations are located directly on the GrIS and measure a series of variables including horizontal wind speed, sensor height and GPS location. The climatic variables are measured every 10 min and thereafter transmitted as hourly averages. The GPS data are recorded every 6 hr. Because the stations are located on the ice sheet where the snowfall accumulation is high, the height above the surface at which the wind speed is measured is variable, as the base of the station is gradually buried under snow during winter. Theoretically, the height measured by the sensor would be 3.1 m if the stations were not to sink into the snow (Fausto *et al.*, 2021). Measured heights above ground, recorded every 6 hr, are provided in the PROMICE datasets. The PROMICE data used in this study are the third version of the hourly datasets of stations QAS_L, QAS_M and QAS_U for the years 2016, 2017 and 2018, except for QAS_M which has only been active since the 11th of August 2016 and which has a very incomplete dataset for 2017. Therefore, only the

2018 dataset was used for this station. This 2016–2018 time period was chosen because, together with the DMI stations, it has the most complete datasets for the selected stations.

The DMI stations (ANG, IKM, IKS, NAR, NUN and UKI; see Table 1) are located on the ice-free area surrounding the GrIS. In Figure 2, some stations seem to be located directly in the ocean. This is due to their location on small islands along the coast that are not resolved by MAR at a 15 km resolution. These stations automatically record variables including wind speed, measured at 10 m a.g.l. every 10 min (Cappelen *et al.*, 2001). The datasets in the chosen time period were available for 2016, 2017 and 2018 for ANG, IKM, NUN and UKI, for 2016 and 2017 for IKS and were only available for 2018 for station NAR. For these stations, the wind gust data (mean highest 3-s wind speed over the past hour, measured at 10 m a.g.l.) was also available.

## 3.3 | The MAR model

MAR is a 3D atmosphere-snowpack regional climate model coupled with the 1D SISVAT (Soil Ice Snow Vegetation Atmosphere Transfer) scheme which enables the modelling of surface processes (Gallée *et al.*, 2013; Fettweis *et al.*, 2017). A full description of the atmospheric part of MAR can be found in Gallée and Schayes (1994). The SISVAT scheme is described in De Ridder and Gallée (1998). A summary of the different modules and schemes used in MAR can be found in Fettweis *et al.* (2017). MAR has been used in multiple studies conducted over Greenland, especially for surface mass balance and surface melt

investigation (e.g., Franco *et al.*, 2012; 2013; Fettweis *et al.*, 2013; 2017; 2020; Hanna *et al.*, 2021; Payne *et al.*, 2021). Its wind speed outputs have been studied over Greenland (Radu *et al.*, 2019; Delhasse *et al.*, 2020) and Antarctica (Gallée and Schayes, 1994; Gallée *et al.*, 2013) but have never been evaluated against in situ observations over the Greenlandic tundra. In this study, the MAR 3.12 version is used. With respect to version 3.11 described in detail in Kittel *et al.* (2021) and Amory *et al.* (2021), MAR v3.12 now uses the standard polar stereographic projection EPSG 3413, corrects an important bug impacting the snow temperature at the base of the snowpack, imposes the conservation of water mass in the soil impacting notably water fluxes over the tundra and uses a continuous conversion from rainfall to snowfall from 0 to −2°C as input of the snow model instead as a fixed one of −1°C.

As being an RCM, MAR needs to be forced with a large-scale model output such as reanalysis or ESM outputs. Large-scale conditions are prescribed every 6 hr at the MAR boundaries (temperature, specific humidity, zonal and meridional wind speeds) at each vertical level and at the surface level (pressure, sea surface temperature and sea ice concentration). A supplementary nudging is applied at the top of the atmosphere by forcing MAR with temperature and wind fields from the large-scale model in the stratosphere (Agosta *et al.*, 2019).

## 3.4 | MAR simulations, reanalysis and ESM outputs

For the evaluation of its wind speed outputs, the sub-region of the study area (see Figure 2) was extracted from MAR simulations run at 15 km resolution from 2015 to 2021 at an hourly scale over the whole of Greenland. 2015 was considered as spin-up. With the aim of validating, MAR was 6 hourly forced with the ERA-5 reanalysis which is the fifth generation of global atmospheric reanalyses produced by the European Centre of Medium-Range Weather

Forecasts (ECMWF; Hersbach *et al.*, 2020). In contrast to its predecessors ERA-40 and ERA-Interim, ERA-5 has a finer spatial resolution (31 km compared with 80 km for ERA-Interim), hourly outputs and more vertical layers (137 extending from surface to 0.01 hPa pressure level). The ERA-5 products, which are updated every 3 months, are currently available from 1950 to the present day. This reanalysis was chosen because, according to Delhasse *et al.* (2020), it is the best choice to force initial and boundary conditions of MAR. This simulation will be referred to as MAR-eval hereafter (see Table 2).

To assess future wind speed and wind power changes, five MAR simulations have been carried out at 15 km resolution over the whole of Greenland at a daily scale with five different forcing fields for 1981–2100 selected from the CMIP6. The subregion of the study area (Figure 2) was extracted thereafter. The ESMs used here as forcing fields are CESM2, CNRM-CM6, CNRM-ESM2, MPI-ESM1-2-HR and UKESM1-0-LL. These ESMs, already used in Hofer *et al.* (2020), were selected for their availability of 6-hourly outputs required to force MAR and their ability to represent the current climate over Greenland as discussed in Hofer *et al.* (2020). From 1981 to 2015, the ESMs were run under the Historical scenario. From 2016 to 2100, their forcing scenario is SSP5-8.5 (O'Neill *et al.*, 2016). This scenario projects an increase in radiative forcing of 8.5 W·m$^{-2}$ by 2100 and has been chosen here to enable the estimation of the extent to which the wind speed field of South Greenland could vary with the largest climate change. To serve as reference for the ESMs forced MAR simulations, a sixth simulation was produced by forcing MAR with ERA-5, this time at a daily scale, from 1981 to 2010 (present). All simulations are summarized in Table 2.

## 3.5 | Evaluation of the MAR wind speed

In order to evaluate the performance of MAR when forced by ERA-5 to simulate wind speed above Cape Farewell, the model outputs have been compared to the

| Time range | Forcing field | Name of simulation | Time step |
|---|---|---|---|
| 2015–2021 | ERA-5 | MAR-eval | Hourly |
| 1981–2010 | ERA-5 | MAR-ERA5-ref | Daily |
| 1981–2100 | CESM2 | MAR-csm | Daily |
| 1981–2100 | CNRM-CM6 | MAR-crmc | Daily |
| 1981–2100 | CNRM-ESM2 | MAR-crme | Daily |
| 1981–2100 | MPI-ESM1-2-HR | MAR-mpi | Daily |
| 1981–2100 | UKESM1-0-LL | MAR-uksm | Daily |

**TABLE 2** List of the different MAR simulations forced with the ensemble of CMIP6 ESMs and the reanalysis ERA-5 used for the evaluation of long-term wind speed variability and validation of MAR. Note the difference in time range between MAR-eval, MAR-ERA5-ref and the other runs

*Note*: The difference in time range between MAR-eval, MAR-ERA5-ref and the other runs.

wind speed observations described in Section 3.2. A methodology, described in Data S1, Supporting Information, was designed to choose the corresponding MAR grid pixel for each station and to check for potential outliers caused by instrumental problems that could alter the results. Statistics for annual and seasonal time series (winter and summer) were then calculated to evaluate MAR. All the results of this evaluation are listed and described in Data S1. To sum up, it appears that even at 15 km of spatial resolution, MAR correlates well with the observations ($R > 0.70$) with relatively small bias and RMSE. On average, the yearly bias is less than 20% of the yearly mean wind speed and the yearly RMSE is less than 1 STD (with exceptions, see the Supplement). However, the MAR performance was locally poorer over the tundra around Cape Farewell, as suggested from the statistics calculated for the stations ANG, KAT_0460 and KAT_6640 because at the resolution of 15 km, MAR is not able to resolve the fjords impacting a lot on the measured wind at these locations. A MAR simulation at higher resolution (5 km) improves the comparison with these stations suggesting that the main bias here is due to the spatial resolution used in this study. Because projections at a resolution of 5 km are too computationally expensive, these had to be run at a coarser resolution leading to the 15 km used here. Finally, the same statistics were computed between hourly wind gust values (3-s highest wind speed) recorded by DMI stations and regular 10 m-modelled wind speed. It turns out that, although slightly underestimated, MAR could capture wind speed maxima at an hourly scale relatively well.

## 3.6 | Methodology of analysis of wind speed anomalies and changes

### 3.6.1 | Spatial wind speed anomalies and changes

Before assessing the two-dimensional future wind speed changes by comparing future mean wind speeds to present ones, the five ESM-forced simulations are evaluated against MAR-ERA5-ref to assess their accuracy in representing the current climate. Annual and seasonal wind speed anomalies of the ESM-forced simulations were computed by comparing them to the reference ERA5-forced simulation over the present climate. Therefore, the 1981–2010 mean wind speeds of the five ESM-forced simulations were compared to the 1981–2010 mean wind speed of MAR-ERA5-ref. The mean wind speeds were calculated at 100 m a.g.l. as it is close to hub height and to the katabatic wind speed maximum of Greenland (Heinemann, 1999). On the other hand, the future wind speed changes (annual and seasonal) were

computed at 100 m a.g.l. as well by comparing the 2071–2100 mean wind speed of each ESM-forced simulation with their corresponding 1981–2010 mean wind speed. The future wind speed changes can be considered significant if their magnitude is greater than the interannual variability, here represented by the 1981–2010 standard deviation of annual or seasonal wind speed. As for ESM-forced wind speed anomalies over current climate, they are considered significant in regard to the 1981–2010 standard deviation of MAR-ERA5-ref. Areas of significant anomaly mean the simulation substantially overestimates (or underestimates) the wind speed compared to the reality.

### 3.6.2 | Time series over 120 years (1981–2100)

In order to quantify the general wind speed change over South Greenland between 1981 and 2100 (annual and seasonal), spatially averaged wind speed changes per grid cell category (ocean, tundra, ice sheet) have been calculated with the help of a linear regression. The mean wind speed of each category was calculated based on an average of all ESM-forced MAR simulations. In addition to quantifying the general wind speed change over South Greenland, the change in maximum wind power that can be yielded by wind turbines was calculated using to the Betz equation described below,

$$P_{\max} = (16/27) \times 0.5 \times \rho \times S \times v^3 \qquad (1)$$

where $P_{\max}$ is the theoretical maximum wind power that a wind turbine can yield in W, $\rho$ is the air density in kg·m$^{-3}$, $S$ is the surface swept by the blade of the turbine in m$^2$ and $v$ is the wind speed in m·s$^{-1}$. The Betz equation was applied to the daily wind speed and air density of each ESM-forced simulation between 1981 and 2100. It should be noted that $S$ has here been fixed to 1.0, thus avoiding any effect relevant to the size of the turbine blade. Once $P_{\max}$ has been calculated for each day, the mean yearly $P_{\max}$ was calculated for each simulation for grid cell categories of tundra and ocean. The ice sheet has not been taken into account here because it is unsuitable terrain for the establishment of on-shore wind turbines.

## 4 | RESULTS

### 4.1 | Spatial wind speed anomalies and changes

The wind speed anomalies between the five ESM-forced simulations and MAR-ERA5-ref are illustrated together
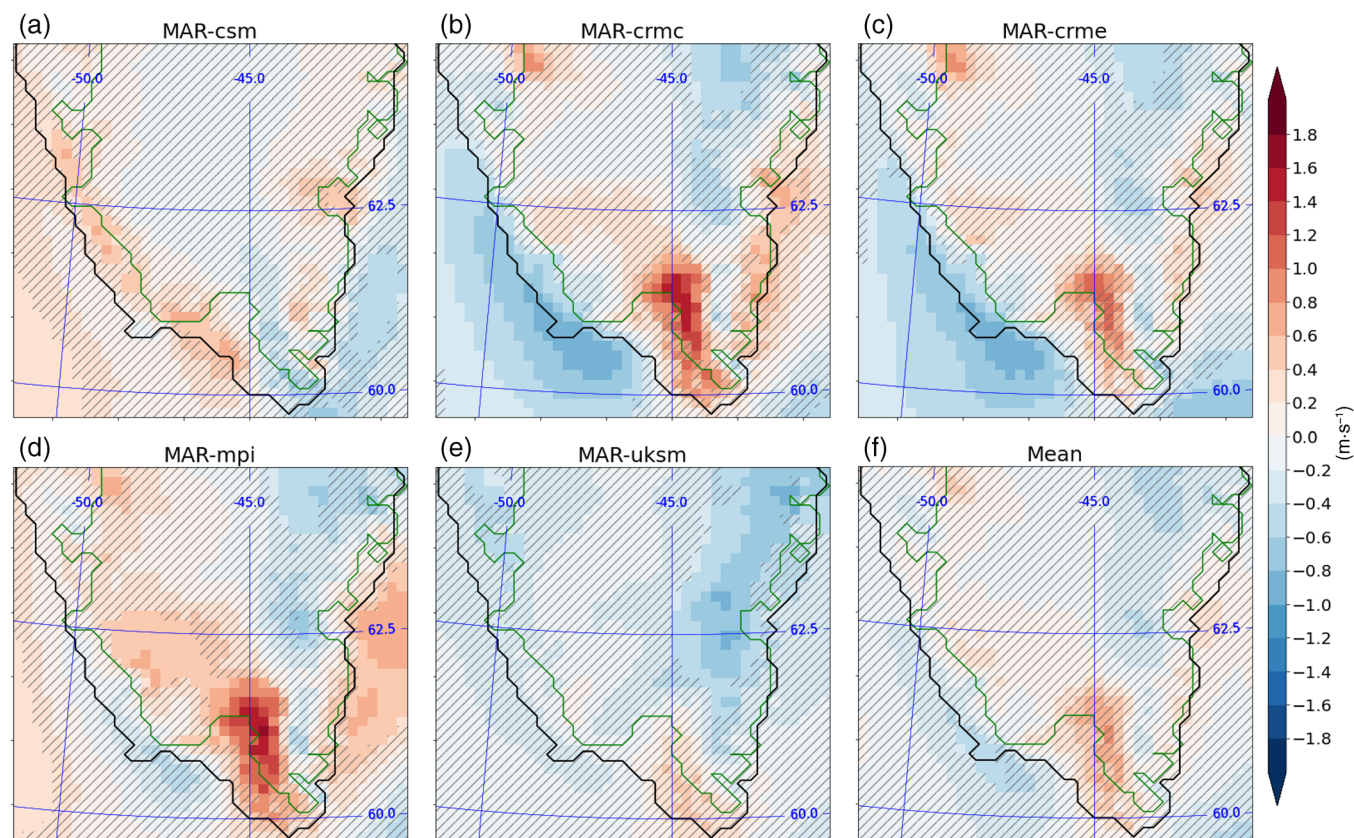
**FIGURE 3** Wind speed anomaly between the five ESM-forced simulations and MAR-ERA5-ref from 1981 to 2010. The hatched area represents the regions where the anomaly is not significant in regard to the interannual variability of MAR-ERA5-ref. The modelled shore line (black), ice sheet contour (green) and longitudes/latitudes (blue) are represented by solid lines. The subplot (f) is the mean anomaly of the five simulations [Colour figure can be viewed at wileyonlinelibrary.com]

with the mean anomaly in Figure 3. The seasonal anomalies (Figures S1 and S2) are similar to the annual anomalies with the greatest (positive) anomaly in magnitude being situated at the very southern tip of Greenland. In general, most of the study area has nonsignificant wind speed anomalies. Moreover, when averaged, these anomalies compensate each other so that the mean anomaly is never significant. This means that the ESM-forced simulations are reliable in representing the current wind speed field and can therefore be considered reliable to simulate the future wind speed field, taking into account the chosen SSP scenario under which they are run.

For the end of this century (2071–2100), MAR projects a significant decrease of mean annual and winter wind speed (Figures 4f and 5f), especially over the tundra on the eastern side of Greenland and over Cape Farewell. Along the western coast, a wind speed decrease is more marked at the winter scale (Figure 5f) than at the annual scale (Figure 4f). On the contrary, MAR projects an increase of the summer wind speed over the ice sheet margins (Figure 6), especially over the western side where significant positive changes are projected (Figure 6f). Finally, at the annual scale, a significant area

of wind speed decrease is noticeable in the middle of the GrIS in Figure 4. This area of decrease is however less clear at the seasonal scale.

## 4.2 | Wind speed and wind power changes between 1981 and 2100

Between 1981 and 2100, the spatially averaged yearly wind speed over the ice sheet, the tundra and the ocean is projected to decrease (Figure 7). The wind speed over the tundra is lower than over the ice sheet because of smaller slopes and higher surface roughness which slow down the katabatic winds flowing down the ice sheet (van den Broeke et al., 1994; Ettema et al., 2010a). A general wind speed decrease, which accentuates around 2020 before stabilizing around 2040, is visually noticeable on all three time series at annual and seasonal scale. This decrease is then projected to strengthen again around 2060 for winter wind speeds until 2080. For this season, the wind speed change is much stronger than in summer, especially over the tundra and the ocean (Figure 7). The quantification of the changes calculated thanks to a linear regression is given in Table 3.
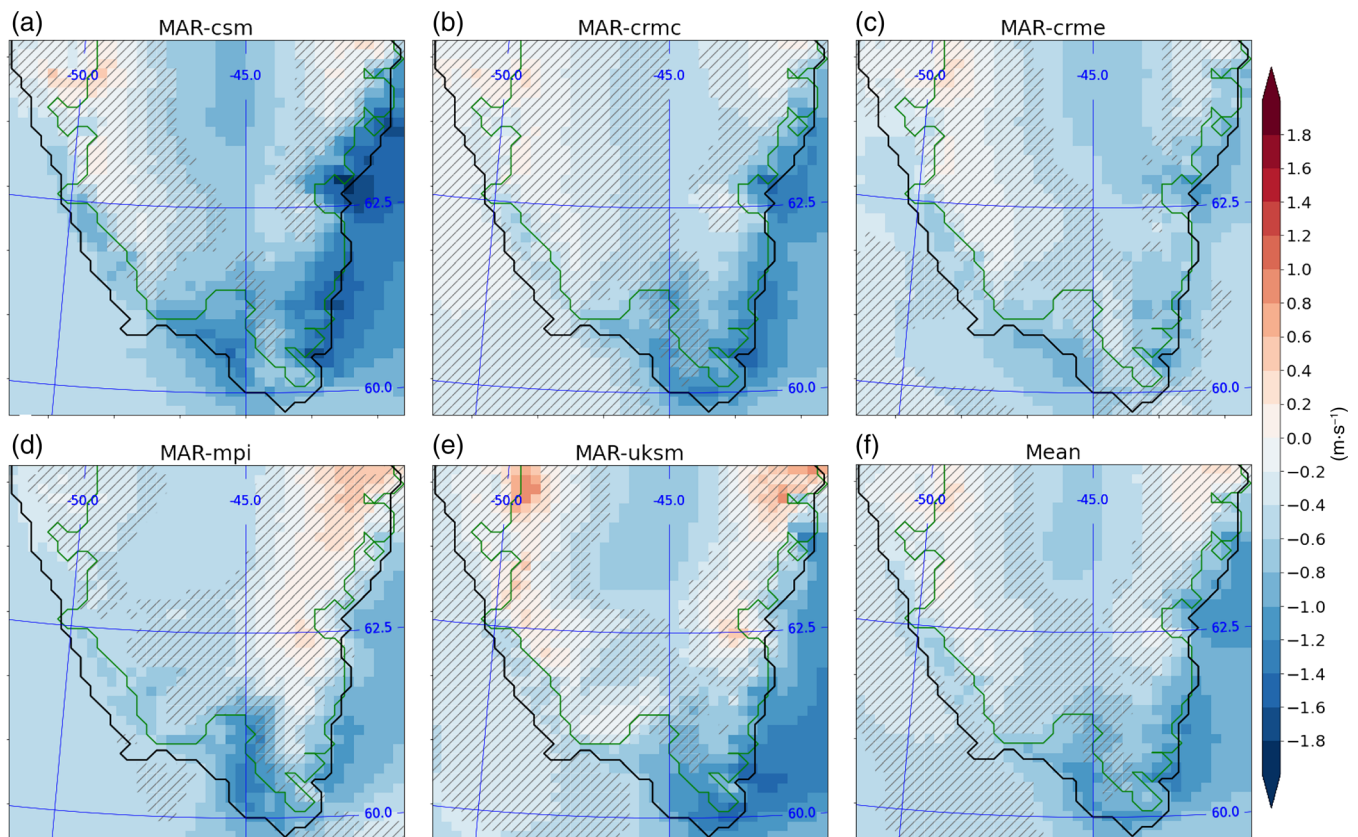
**FIGURE 4** Projected mean yearly wind speed changes from 2071 to 2100 compared to 1981–2010. The hatched part represents the region where the change is insignificant with regard to the yearly present-day interannual variability. The modelled shore line (black), ice sheet contour (green) and longitudes/latitudes (blue) are represented by solid lines. The subplot (f) is the mean anomaly of the five simulations [Colour figure can be viewed at wileyonlinelibrary.com]

Over 120 years from 1981 to 2100, the annual wind speed is suggested to decrease by $\sim-0.7$ m·s$^{-1}$ over the ice sheet and by $\sim-0.8$ m·s$^{-1}$ over the ocean and the tundra. In summer, these numbers are $\sim-0.4$ m·s$^{-1}$ for the ice sheet and the ocean and $\sim-0.3$ m·s$^{-1}$ for the tundra while in winter, the wind speed changes are $\sim-0.6$ m·s$^{-1}$ over the ice sheet, $\sim-1.3$ m·s$^{-1}$ over the ocean and $\sim-0.9$ m·s$^{-1}$ over the tundra. Again, these numbers highlight the stronger winter wind speed decrease over the tundra and the ocean (around 3 times as much as in summer) compared to the ice sheet. The decreasing trends in wind speed can be considered significant ($p$-value $<.001$; see Table 3).

The change in the potential maximum wind power a turbine can yield is shown in Figure 8 for ocean and tundra based on yearly and seasonal values of maximum wind power (the ice sheet has not been considered here as it is unsuitable ground for wind farm establishment). As a reminder, the maximum wind power has been computed from daily values of wind speed and air density. The air density change is not shown here but it is projected to decrease due to rising temperatures over the whole study area. Combined with the decrease in wind speeds, the decrease in air density will lead to a reduction in the maximum wind power (Figure 8). However, MAR projections surprisingly suggest a higher maximum wind power above the tundra than above the ocean despite lower wind speed and smaller density over the tundra than over the ocean. Indeed, the air density is higher over the ocean at 100 m a.g.l., because the elevation of the 100 m level above the surface is lower and the air above it contains more humidity than that above the tundra. This is likely because the Betz equation considers the cubic wind speed and was applied to daily values of wind speed and air density. Although the yearly mean wind speed is, on average, smaller for the tundra than for the ocean, the tundra experiences higher maximum daily wind speeds than the ocean (maximum daily wind speed of 32 m·s$^{-1}$ over the tundra between 1981 and 2010 vs. 25 m·s$^{-1}$ for the ocean). Raised to cubic power, these events would lead to higher yearly wind power values for the tundra. The change of average yearly and seasonal wind power is listed in Table 4. The yearly change over the tundra ($\sim-178.1$ W) is projected to be stronger than over the ocean ($\sim-155.4$ W). This is also the case in
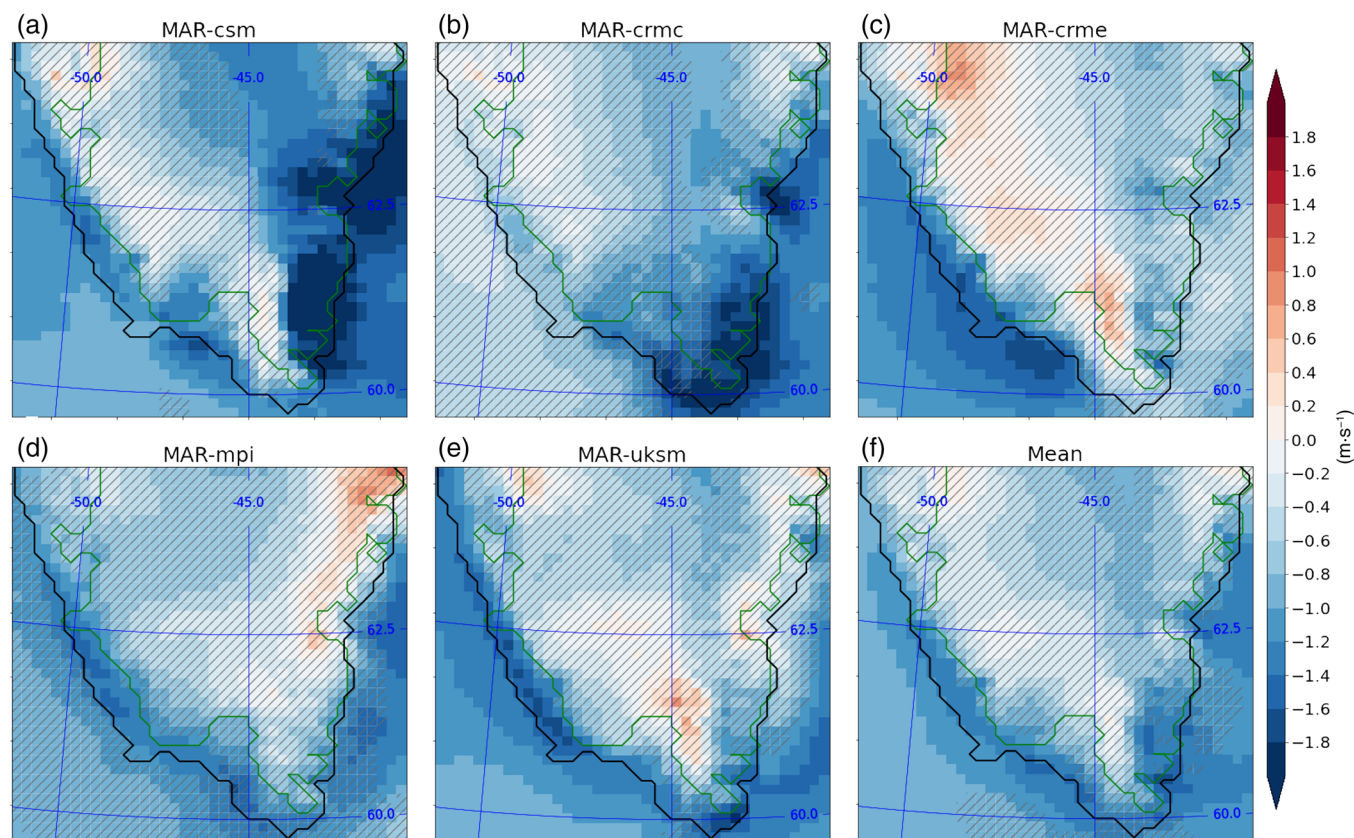
**FIGURE 5** Projected mean winter wind speed changes (DJF) from 2071–2100 compared to 1981–2010. The hatched part represents the region where the change is insignificant with regard to the winter present-day interseasonal variability. The modelled shore line (black), ice sheet contour (green) and longitudes/latitudes (blue) are represented by solid lines. The subplot (f) is the mean anomaly of the five simulations [Colour figure can be viewed at wileyonlinelibrary.com]

summer ($\sim-63.9$ W over the tundra and $\sim-59.5$ W over the ocean). In winter, the change is approximately 4 times stronger than in summer with a decrease of $\sim-268.4$ W over the tundra and $\sim-273.1$ W over the ocean. These changes are significant with regard to their $p$-value. Finally, it appears from Figure 8 that in the summer, the maximum wind power is similar over the tundra and the ocean while, on average, it becomes stronger over the tundra during winter and at the annual scale when compared with the ocean.

## 5 | DISCUSSION

A general wind speed decrease is projected over South Greenland by the end of the 21st century. This decrease is exacerbated in winter while in summer, areas of increased wind speed could occur along the ice sheet margins, especially on the west side. A complementary analysis of wind speed change at different vertical levels (10 m, 50 m, 500 hPa; Figure S3) suggests that the wind speed reduction found at 100 m a.g.l. is mainly induced

by a reduction in synoptic wind speed. At 500 hPa, all simulations agree on a wind speed decrease in winter, as indicated in Figure S3i where significant decrease is found. This general wind speed decrease could be explained by the Arctic amplification. The enhanced warming in the Arctic caused by the ice albedo feedback induces an attenuation of the meridional temperature gradient between the mid-latitudes and the Poles (Jung and Schindler, 2019). However, this temperature gradient is driving the large-scale atmospheric circulation of the Northern Hemisphere so its weakening would lead to a slowing down of the synoptic dominant winds (Jung and Schindler, 2019). During winter, the large-scale temperature gradient is stronger than in summer (leading to higher wind speeds) but with the decreasing insulating sea ice cover, the ocean releases more and more heat (absorbed during sunny days) into the cold atmosphere, enhancing the weakening of the gradient by warming the air during this season (Serreze and Francis, 2006). This would explain why the expected wind speed decrease is stronger in winter. In summer however, the simulations disagree whether the wind
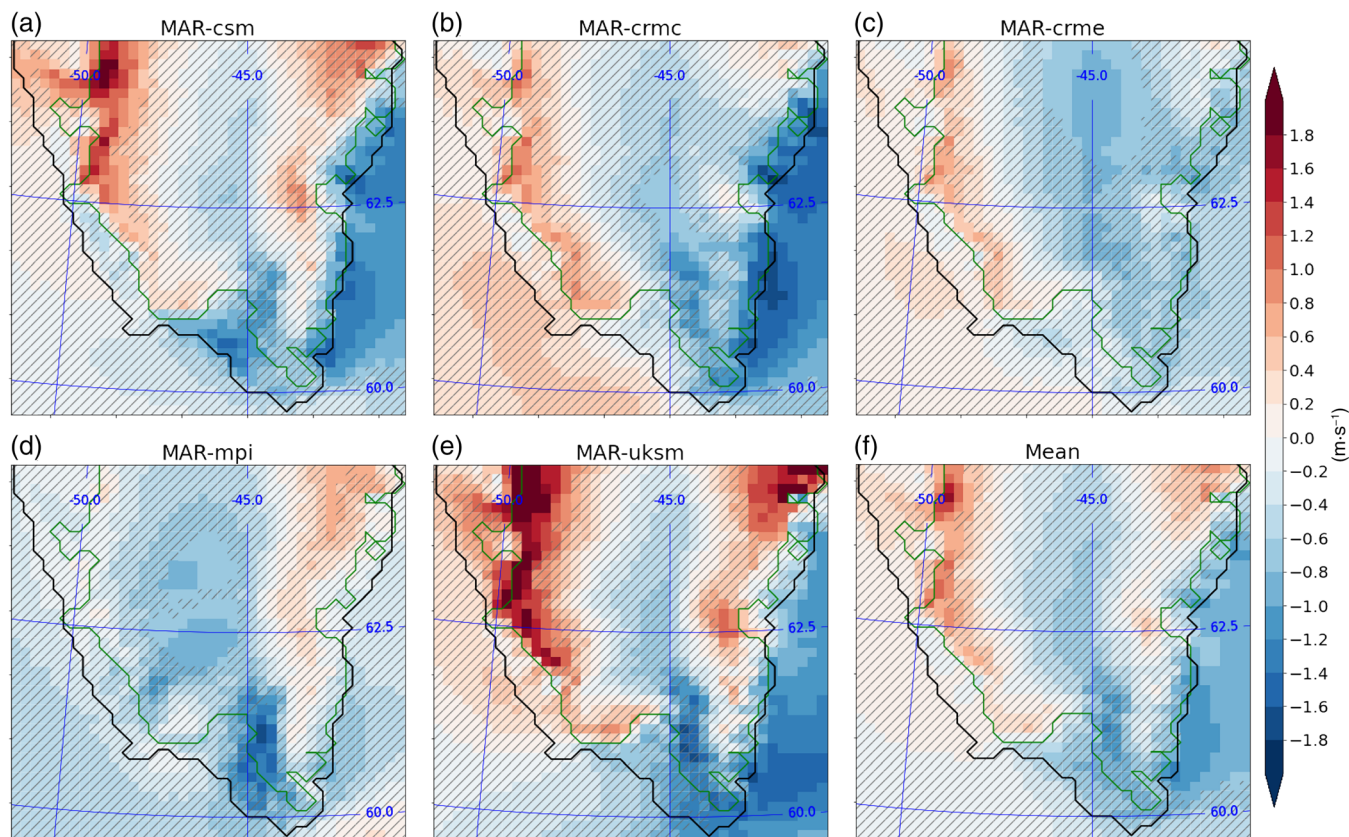
**FIGURE 6** Projected mean summer wind speed changes (JJA) from 2071–2100 compared to 1981–2010. The hatched part represents the region where the change is insignificant with regard to the summer present-day interseasonal variability. The modelled shore line (black), ice sheet contour (green) and longitudes/latitudes (blue) are represented by solid lines. The subplot (f) is the mean anomaly of the five simulations [Colour figure can be viewed at wileyonlinelibrary.com]

speed increases or decreases at 500 hPa so the evidence of synoptic wind speed decrease is less clear for this season. If there is no more sea ice cover left during summer due to global warming under scenario SSP5-8.5, the large-scale temperature gradient is no longer influenced by sea surface albedo changes during this season. The link between the projected rising air temperature and decreasing wind speeds is supported by Figure 9 in which all simulations agree that a higher yearly temperature anomaly at 500 hPa correlates with an amplified negative yearly wind speed anomaly at 100 m a.g.l.

Furthermore, the increase in summer wind speed at the edges of the ice sheet margins by 2100 can be explained by the strengthening of the air temperature gradient between the tundra and the ice sheet. With global warming, the temperature over the tundra is projected to increase over time while the temperature of the ice sheet cannot rise above melting point. Over the ablation zone of the ice sheet, the air is cooled by the melting snow and ice. On the contrary, the heating

of the air above the tundra is not limited by the presence of snow or ice during summer, reinforcing the temperature contrast between the two areas (Franco et al., 2013; Gorter et al., 2014). Figure 10 displays the 30-year mean air temperature change simulated by MAR between 1981–2010 and 2071–2100. The rise of the temperature at 2 m a.g.l. is limited over the ice sheet margins while it reaches approximately +5°C over the tundra under emission scenario SSP5-8.5. As explained in Section 2, the temperature gradient between the ice sheet and the surrounding tundra generates a horizontal pressure gradient that drives the formation of katabatic winds. As a consequence of this gradient strengthening, the katabatic forcing above the ice sheets edges is stronger and leads to higher wind speeds in summer.

Although at 100 m a.g.l., areas of wind speed decrease in summer are not significant, at 10 m a.g.l., a marginally significant wind speed decrease is noticeable in the middle of the ice sheet (Figure S3b). This might be explained by a small reduction in the katabatic forcing induced by
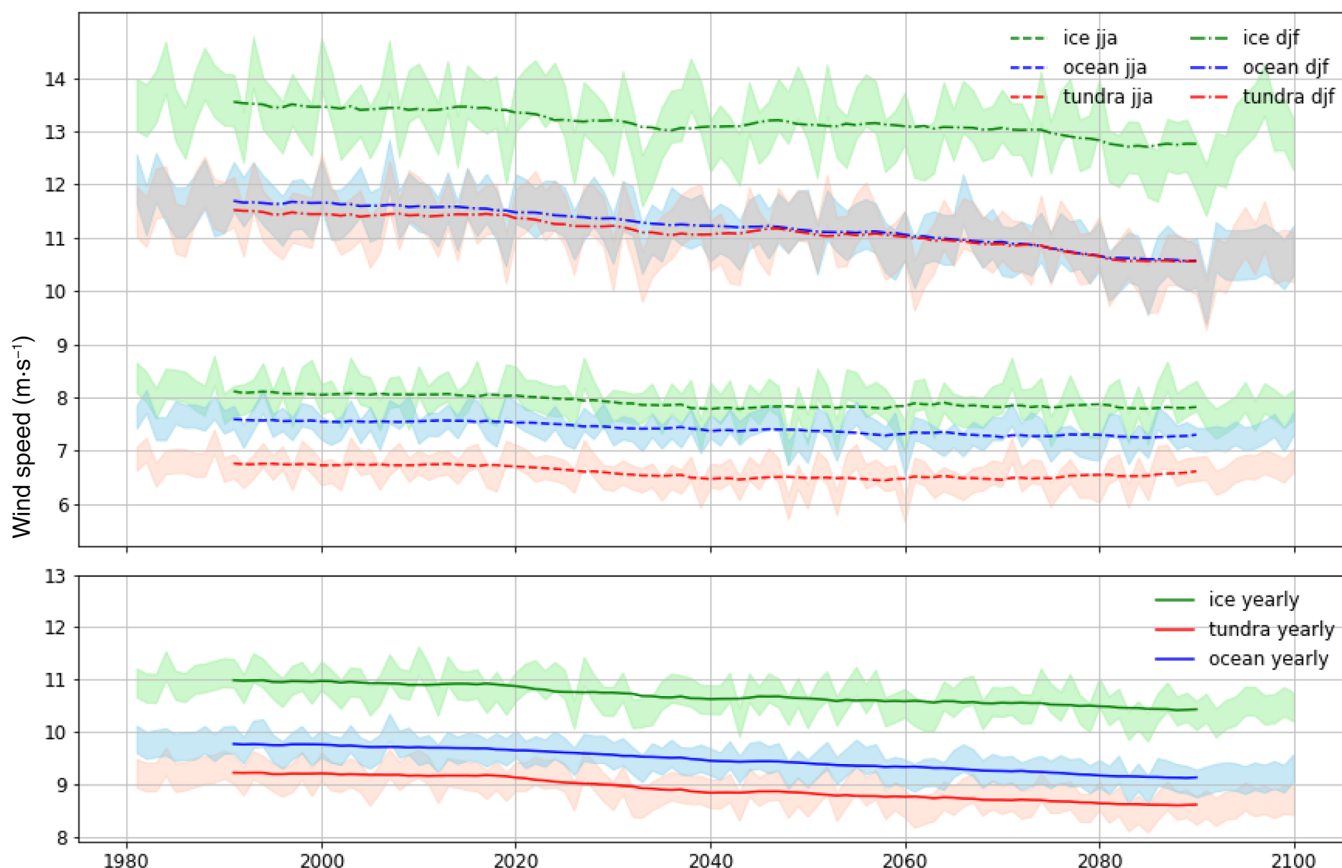
**FIGURE 7**    Wind speed time series between 1981 and 2100 averaged over the ice sheet (green), the ocean (blue) and the tundra (red). A 10-year rolling mean has been applied to the time series. Solid, dashed and dash dotted lines respectively represent the yearly, summer (JJA) and winter (DJF) wind speed. The coloured bands represent the interannual variability [Colour figure can be viewed at wileyonlinelibrary.com]

**TABLE 3**    Projected seasonal and yearly wind speed changes between 1981 and 2100 over ice sheet, ocean and tundra, yearly *standard deviation (SD)* and *p*-value of the change

| Time period | Grid cell category | Mean wind speed of 1981–2010 (m·s⁻¹) | Wind speed change (m·s⁻¹) | SD (m·s⁻¹) | p-value |
|---|---|---|---|---|---|
| JJA | Ice sheet | 8.09 | −0.38 | 0.28 | <.001 |
| JJA | Ocean | 7.57 | −0.40 | 0.22 | <.001 |
| JJA | Tundra | 6.76 | −0.27 | 0.22 | <.001 |
| DJF | Ice sheet | 13.51 | −0.84 | 0.49 | <.001 |
| DJF | Ocean | 11.68 | −1.34 | 0.46 | <.001 |
| DJF | Tundra | 11.48 | −1.09 | 0.47 | <.001 |
| Yearly | Ice sheet | 10.97 | −0.67 | 0.28 | <.001 |
| Yearly | Ocean | 9.76 | −0.80 | 0.26 | <.001 |
| Yearly | Tundra | 9.21 | −0.77 | 0.27 | <.001 |

an increase in surface roughness. With the temperature rising, the ice sheet would experience more melt and thus have more run-off water flowing over it (Fettweis *et al.*, 2017). In the upper part of the ice sheet, mostly covered in snow where the surface roughness is less than

in the ablation zone, this increased surface run-off would enhance the surface roughness as parametrized in MAR and slow down the katabatic winds by creating drainage channels (Greuell and Konzelmann, 1994; Lefebre *et al.*, 2003).
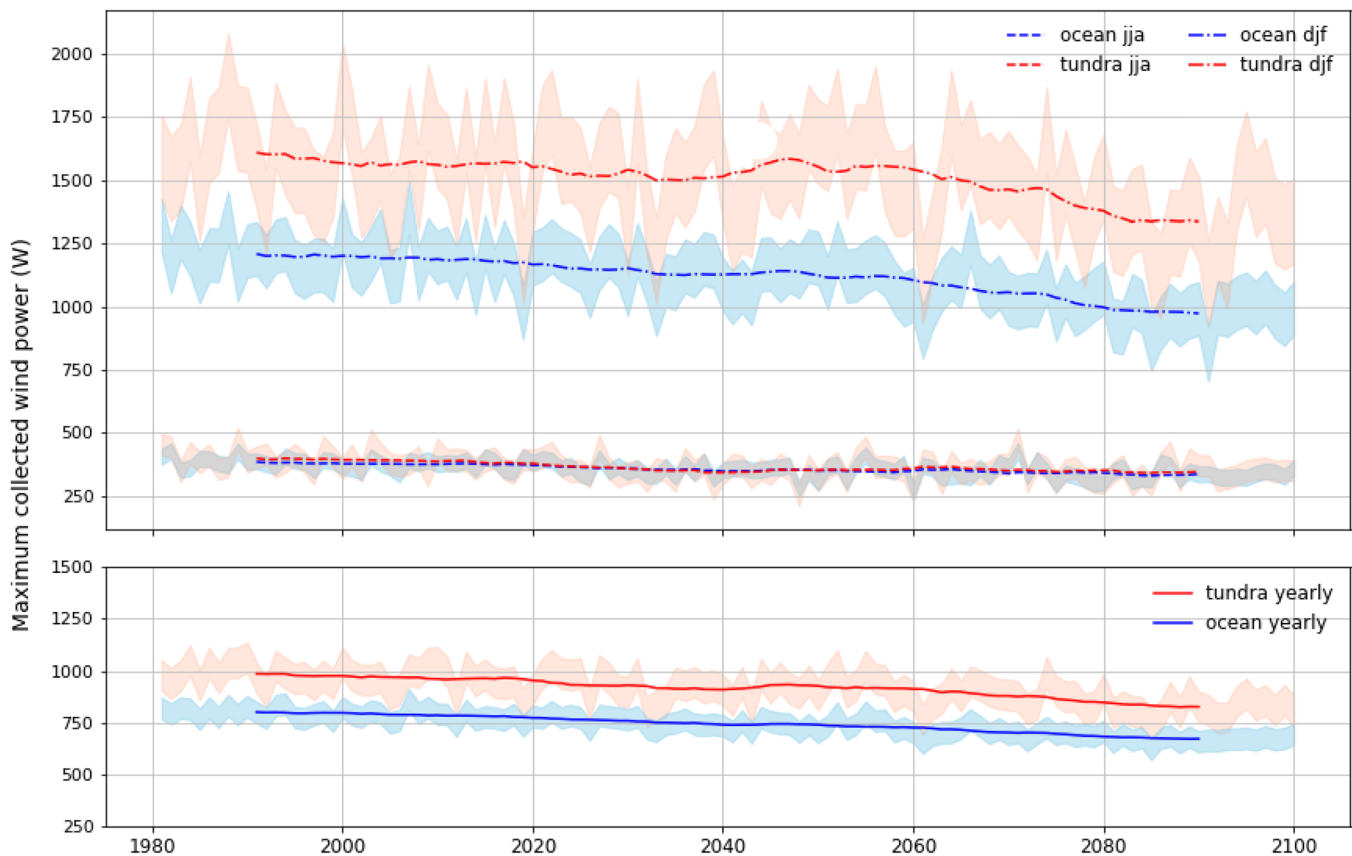
**FIGURE 8** Maximum wind power that can be collected by a turbine between 1981 and 2100 over ocean (blue) and tundra (red), calculated with the Betz equation where the surface swept by the blade of the turbine has been set to 1.0. A 10-year rolling mean has been applied to the time series. Solid, dashed and dash dotted lines, respectively, represent the yearly, summer (JJA) and winter (DJF) maximum wind power. The coloured bands represent the interannual variability [Colour figure can be viewed at wileyonlinelibrary.com]

**TABLE 4** Projected yearly and seasonal maximum collected wind power change between 1981 and 2100 over ocean and tundra, yearly *SD* and *p*-value of the change

| Time period | Grid cell category | Mean maximum wind power of 1981–2010 (W) | Wind power change (W) | *SD* (W) | *p*-value |
|---|---|---|---|---|---|
| JJA | Ocean | 381.25 | −59.49 | 31.32 | <.001 |
| JJA | Tundra | 396.89 | −63.88 | 42.39 | <.001 |
| DJF | Ocean | 1207.19 | −273.13 | 106.21 | <.001 |
| DJF | Tundra | 1590.78 | −268.37 | 168.44 | <.001 |
| Yearly | Ocean | 801.04 | −155.35 | 51.63 | <.001 |
| Yearly | Tundra | 983.20 | −178.08 | 73.82 | <.001 |

Considering these findings, the decreasing wind speed in winter by 2100 could be beneficial for renewable electricity production. During this season, very high wind speeds (up to 30 m·s$^{-1}$ on average) occur over the tundra in South Greenland which can exceed the cut-out speed of wind turbines (about 25 m·s$^{-1}$ but it depends on the turbine model), leading to discontinuous energy production (Radu *et al.*, 2019). The projected winter wind speed trend suggests that the cut-out speed threshold would be less and less often surpassed (although in the future, improvements in wind turbines technology might avoid this wintertime energy-generation disruption). However, one limitation of this study is that projected wind speed trends have been investigated on seasonally and annually averaged wind speeds. To assess this hypothesis, an analysis of the occurrence of extreme wind speed events by
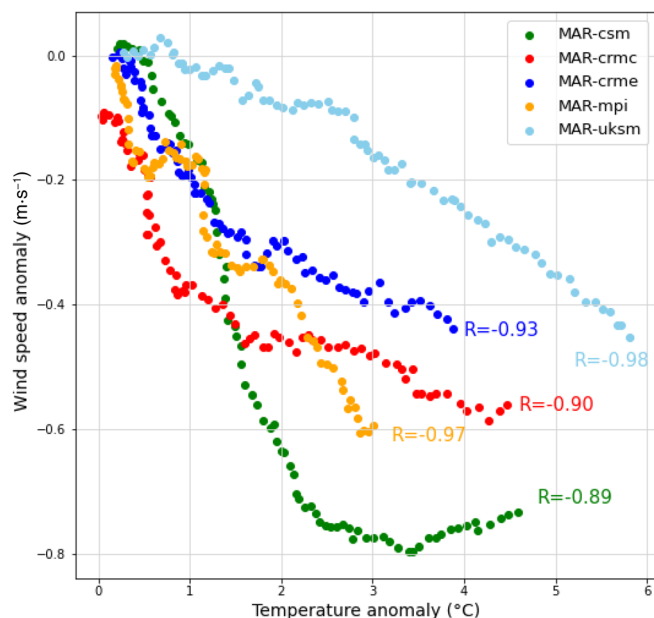
**FIGURE 9** Projected yearly wind speed anomalies (with regard to the 1981–2010 mean wind speed) at 100 m a.g.l. versus the projected yearly air temperature anomalies at 500 hPa (with regard to the 1981–2010 mean air temperature) of each ESM-forced simulation between 1981 and 2010. A 20-year rolling mean has been applied on the wind speed anomaly and temperature anomaly time series [Colour figure can be viewed at wileyonlinelibrary.com]
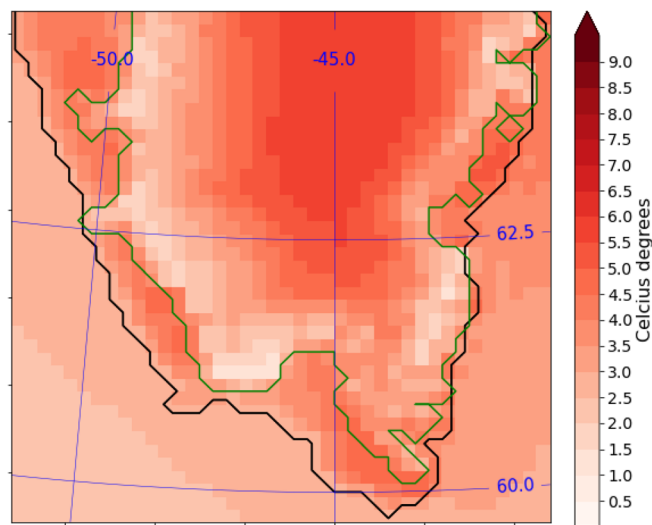


**FIGURE 10** Projected mean air temperature change at 2 m a.g.l. between 1981–2010 and 2071–2100, derived from an average of five ESM-forced simulations of MAR under emission scenario SSP5-8.5. The modelled shore line (black), ice sheet contour (green) and longitudes/latitudes (blue) are represented by solid lines [Colour figure can be viewed at wileyonlinelibrary.com]

the end of the 21st century should be conducted with regard to the cut-out speed threshold overtaking of wind turbines and is suggested as further work. Moreover, the daily wind speeds that might lead to wind turbines cut-

off have not been removed from the times series used to calculate the potential maximum wind power with the Betz Equation (1).

## 6 | CONCLUSIONS

This work has aimed to answer how the wind speed over South Greenland is expected to change by 2100. Therefore, an evaluation of MAR was first performed by comparing its hourly wind speed outputs at 15 km with observations from KATABATA, DMI and PROMICE automatic weather stations in order to assess the model reliability to simulate wind speeds over the tundra in South Greenland. It turned out that MAR could accurately represent wind speed at that time and spatial resolution, although the smoothing of the topography by the model resolution used here (15 km) induced some significant local biases over the tundra.

As for the investigation of future wind speed changes, it was found that a general wind speed decrease is projected to occur by 2100 over South Greenland. This decrease might be primarily explained by a weakening of the Northern Hemisphere meridional temperature gradient that drives large-scale atmospheric circulation as a consequence of the Arctic amplification. Nonetheless in summer, because the ice temperature cannot rise above melting point, cooling its subjacent air-layers, the katabatic forcing is likely increased at the ice sheet margins. With greater temperature contrasts between the tundra and ice sheet in summer, the pressure gradient driving katabatic wind formation is reinforced.

Despite an increase in katabatic winds in the summer, it is still projected that the wind energy that can be collected by wind turbines during this season will be less, even if not by a large amount, in 2100 than nowadays. However, it is projected that this decrease in wind energy collected will be approximately 4 times stronger in the winter that in the summer. We note that this decrease in wind energy production is caused both by a decrease in wind speed and in air density.

In light of the findings from this study, further investigation should be conducted about the effects these projected changes in wind speed over the Greenlandic tundra might have on effective and efficient wind turbine functioning. Nonetheless, the projected wind speed decrease in winter might be beneficial for wind turbines as it suggests less frequent high wind speeds that might negatively affect the electricity production by cutting off the turbines. This should however be investigated deeper in detail by analysing long-term trends of high wind speeds frequency, while taking into account the

continuous developments in wind turbine technology to increase their cut-out speed.

## CONFLICT OF INTEREST
The authors declare no potential conflict of interest.

## DATA AVAILABILITY STATEMENT
The main KATABATA hourly measurement as well as the main MAR outputs are available on Zenodo (https://doi.org/10.5281/zenodo.6055786) and the modelled datasets presented in this study are also available from the authors upon request and without conditions. Data from the Programme for Monitoring of the Greenland Ice Sheet (PROMICE) were provided by the Geological Survey of Denmark and Greenland (GEUS) at http://www.promice.dk and were downloaded on October 25, 2021 from https://promice.org/PromiceDataPortal/api/download/f24019f7-d586-4465-8181-d4965421e6eb/v3/hourly/csv. Data from the Danish Meteorological Institute were downloaded from https://dmiapi.govcloud.dk/ on October 20, 2021.

## ORCID
*Clara Lambin* https://orcid.org/0000-0002-4763-8744
*Christoph Kittel* https://orcid.org/0000-0001-6586-9784

## REFERENCES
Agosta, C., Amory, C., Kittel, C., Orsi, A., Favier, V., Gallée, H., van den Broeke, M.R., Lenaerts, J., van Wessem, J.M., van de Berg, W.J., and Fettweis, X. (2019) Estimation of the Antarctic surface mass balance using the regional climate model MAR (1979–2015) and identification of dominant processes. *Cryosphere*, 13, 281–296.

Amory, C., Kittel, C., Le Toumelin, L., Agosta, C., Delhasse, A., Favier, V. and Fettweis, X. (2021) Performance of MAR (v3. 11) in simulating the drifting-snow climate and surface mass balance of Adelie land, East Antarctica. *Geoscientific Model Development*, 14, 3487–3510.

Berger, M., Radu, D.C., Detienne, G., Deschuyteneer, T., Richel, A. and Ernst, D. (2021) Remote renewable hubs for carbonneutral synthetic fuel production. *Frontiers in Energy Research*, 9, 1–22.

Bromwich, D.H., Cassano, J.J., Klein, T., Heinemann, G., Hines, K. M., Steffen, K. and Box, J.E. (2001) Mesoscale modeling of katabatic winds over Greenland with the Polar MM5. *Monthly Weather Review*, 129, 2290–2309.

Cappelen, J., Jørgensen, B.V., Laursen, E.V., Stannius, L.S. and Thomsen, R.S. (2001) *The observed climate of Greenland, 1958–99: with climatological standards normals, 1961–90.* Copenhagen: Danish Meteorological Institute, Ministery of Transport. Technical report: 00-18.

Chatzivasileiadis, S., Ernst, D. and Andersson, G. (2013) The global grid. *Renewable Energy*, 57, 372–383.

da Silva Soares, J. P. (2016) *Wind energy utilizationin arctic climate-RACMO 2.3 Greenland climate runs project.* Master's thesis, Uppsala University, Sweden.

De Ridder, K. and Gallée, H. (1998) Land surface–induced regional climate change in southern Israel. *Journal of Applied Meteorology*, 37, 1470–1485.

Delhasse, A., Kittel, C., Amory, C., Hofer, S., van As, D., Fausto, R. S. and Fettweis, X. (2020) Brief communication: evaluation of the near-surface climate in ERA5 over the Greenland ice sheet. *Cryosphere*, 14, 957–965.

Ettema, J., van den Broeke, M.R., van Meijgaard, E. and Van de Berg, W.J. (2010a) Climate of the Greenland ice sheet using a high-resolution climate model—part 2: near-surface climate and energy balance. *Cryosphere*, 4, 529–544.

Ettema, J., van den Broeke, M.R., van Meijgaard, E., Van de Berg, W.J., Box, J.E. and Steffen, K. (2010b) Climate of the Greenland ice sheet using a high-resolution climate model—part 1: evaluation. *Cryosphere*, 4, 511–527.

Fausto, R.S., van As, D., Mankoff, K.D., Vandecrux, B., Citterio, M., Ahlstrøm, A.P., Andersen, S.B., Colgan, W., Karlsson, N.B., Kjeldsen, K.K., Korsgaard, N.J., Larsen, S.H., Nielsen, S., Pedersen, A.Ø., Shields, C.L., Solgaard, A.M. and Box, J.E. (2021) Programme for Monitoring of the Greenland Ice Sheet (PROMICE) automatic weather station data. *Earth System Science Data*, 13, 3819–3845.

Fettweis, X., Box, J.E., Agosta, C., Amory, C., Kittel, C., Lang, C., van As, D., Machguth, H. and Gallée, H. (2017) Reconstructions of the 1900–2015 Greenland ice sheet surface mass balance using the regional climate mar model. *Cryosphere*, 11, 1015–1033.

Fettweis, X., Franco, B., Tedesco, M., Van Angelen, J.H., Lenaerts, J.T.M., van den Broeke, M.R. and Gallée, H. (2013)

Estimating the Greenland ice sheet surface mass balance contribution to future sea level rise using the regional atmospheric climate model MAR. *Cryosphere*, 7, 469–489.

Fettweis, X., Hofer, S., Krebs-Kanzow, U., Amory, C., Aoki, T., Berends, C.J., Born, A., Box, J.E., Delhasse, A., Fujita, K., Gierz, P., Goelzer, H., Hanna, E., Hashimoto, A., Huybrechts, P., Kapsch, M.L., King, M.D., Kittel, C., Lang, C., Langen, P.L., Lenaerts, J.T.M., Liston, G.E., Lohmann, G., Mernild, S.H., Mikolajewicz, U., Modali, K., Mottram, R.H., Niwano, M., Noël, B., Ryan, J.C., Smith, A., Streffing, J., Tedesco, M., van de Berg, W.J., van den Broeke, M., van de Wal, R.S.W., van Kampenhout, L., Wilton, D., Wouters, B., Ziemen, F. and Zolles, T. (2020) GrSMBMIP: intercomparison of the modeled 1980–2012 surface mass balance over the Greenland Ice Sheet. *Cryosphere*, 14, 3935–3958.

Franco, B., Fettweis, X. and Erpicum, M. (2013) Future projections of the Greenland ice sheet energy balance driving the surface melt. *Cryosphere*, 7, 1–18.

Franco, B., Fettweis, X., Lang, C. and Erpicum, M. (2012) Impact of spatial resolution on the modelling of the Greenland ice sheet surface mass balance between 1990–2010, using the regional climate model MAR. *Cryosphere*, 6, 695–711.

Gallée, H. and Schayes, G. (1994) Development of a three-dimensional meso-γ primitive equation model: katabatic winds simulation in the area of Terra Nova Bay, Antarctica. *Monthly Weather Review*, 122, 671–685.

Gallée, H., Trouvilliez, A., Agosta, C., Genthon, C., Favier, V. and Naaim-Bouvet, F. (2013) Transport of snow by the wind: a comparison between observations in Adélie Land, Antarctica, and simulations made with the regional climate model MAR. *Boundary-Layer Meteorology*, 146, 133–147.

Gorter, W., Van Angelen, J.H., Lenaerts, J.T.M. and van den Broeke, M.R. (2014) Present and future near-surface wind climate of Greenland from high resolution regional climate modelling. *Climate Dynamics*, 42, 1595–1611.

Greuell, W. and Konzelmann, T. (1994) Numerical modelling of the energy balance and the englacial temperature of the Greenland Ice Sheet. Calculations for the ETH-Camp location (West Greenland, 1155 m asl). *Global and Planetary Change*, 9, 91–114.

Hanna, E., Cappelen, J., Fettweis, X., Mernild, S.H., Mote, T.L., Mottram, R., Steffen, K., Ballinger, T.J. and Hall, R.J. (2021) Greenland surface air temperature changes from 1981 to 2019 and implications for ice-sheet melt and mass-balance change. *International Journal of Climatology*, 41, E1336–E1352.

Heinemann, G. (1999) The KABEG'97 field experiment: an aircraft-based study of katabatic wind dynamics over the Greenland ice sheet. *Boundary-Layer Meteorology*, 93, 75–116.

Hersbach, H., Bell, B., Berrisford, P., Hirahara, S., Horányi, A., Muñoz-Sabater, J., Nicolas, J., Peubey, C., Radu, R., Schepers, D., Simmons, A., Soci, C., Abdalla, S., Abellan, X., Balsamo, G., Bechtold, P., Biavati, G., Bidlot, J., Bonavita, M., Chiara, G., Dahlgren, P., Dee, D., Diamantakis, M., Dragani, R., Flemming, J., Forbes, R., Fuentes, M., Geer, A., Haimberger, L., Healy, S., Hogan, R.J., Hólm, E., Janisková, M., Keeley, S., Laloyaux, P., Lopez, P., Lupu, C., Radnoti, G., Rosnay, P., Rozum, I., Vamborg, F., Villaume, S. and Thépaut, J.N. (2020) The ERA5 global reanalysis. *Quarterly Journal of the Royal Meteorological Society*, 146, 1999–2049.

Hofer, S., Lang, C., Amory, C., Kittel, C., Delhasse, A., Tedstone, A. and Fettweis, X. (2020) Greater Greenland Ice Sheet contribution to global sea level rise in CMIP6. *Nature Communications*, 11, 1–11.

Jakobsen, K. R. (2016) *Renewable energy potential of Greenland with emphasis on wind resource assessment*. PhD thesis, Technical University of Denmark, Lyngby, Denmark.

Jung, C. and Schindler, D. (2019) Changing wind speed distributions under future global climate. *Energy Conversion and Management*, 198, 111841.

Kittel, C., Amory, C., Agosta, C., Jourdain, N.C., Hofer, S., Delhasse, A., Doutreloup, S., Huot, P.-V., Lang, C., Fichefet, T. and Fettweis, X. (2021) Diverging future surface mass balance between the Antarctic ice shelves and grounded ice sheet. *Cryosphere*, 15, 1215–1236.

Klein, T. and Heinemann, G. (2002) Interaction of katabatic winds and mesocyclones near the eastern coast of Greenland. *Meteorological Applications*, 9, 407–422.

Klein, T., Heinemann, G., Bromwich, D.H., Cassano, J.J. and Hines, K.M. (2001) Mesoscale modeling of katabatic winds over Greenland and comparisons with aws and aircraft data. *Meteorology and Atmospheric Physics*, 78, 115–132.

Lefebre, F., Gallée, H., van Ypersele, J.-P. and Greuell, W. (2003) Modeling of snow and ice melt at ETH Camp (West Greenland): a study of surface albedo. *Journal of Geophysical Research: Atmospheres*, 108, 4231.

Moore, G.W.K. and Renfrew, I.A. (2005) Tip jets and barrier winds: a QuikSCAT climatology of high wind speed events around Greenland. *Journal of Climate*, 18, 3713–3725.

Moore, G.W.K., Renfrew, I.A., Harden, B.E. and Mernild, S.H. (2015) The impact of resolution on the representation of Southeast Greenland barrier winds and katabatic flows. *Geophysical Research Letters*, 42, 3011–3018.

O'Neill, B.C., Tebaldi, C., van Vuuren, D.P., Eyring, V., Friedlingstein, P., Hurtt, G., Knutti, R., Kriegler, E., Lamarque, J.-F., Lowe, J., Meehl, G. A., Moss, R., Riahi, K. and Sanderson, B. M. (2016) The scenario model intercomparison project (ScenarioMIP) for CMIP6. *Geoscientific Model Development*, 9, 3461–3482.

Payne, A.J., Nowicki, S., Abe-Ouchi, A., Agosta, C., Alexander, P., Albrecht, T., Asay-Davis, X., Aschwanden, A., Barthel, A., Bracegirdle, T.J., Calov, R., Chambers, C., Choi, Y., Cullather, R., Cuzzone, J., Dumas, C., Edwards, T.L., Felikson, D., Fettweis, X., Galton-Fenzi, B.K., Goelzer, H., Gladstone, R.R.M., Golledge, N.R., Gregory, J.M., Greve, R., Hattermann, T., Hoffman, M.J., Humbert, A., Huybrechts, P., Jourdain, N.C., Kleiner, T., Munneke, P.K., Larour, E., Le clec'h, S., Lee, V., Leguy, G., Lipscomb, W.H., Little, C.M., Lowry, D.P., Morlighem, M., Nias, I., Pattyn, F., Pelle, T., Price, S.F., Quiquet, A., Reese, R., Rückamp, M., Schlegel, N., Seroussi, H., Shepherd, A., Simon, E., Slater, D., Smith, R.S., Straneo, F., Sun, S., Tarasov, L., Trusel, L.D., Van Breedam, J., van de Wal, R., van den Broeke, M., Winkelmann, R., Zhao, C., Zhang, T., and Zwinger, T. (2021) Future sea level change under CMIP5 and CMIP6 scenarios from the Greenland and Antarctic ice sheets. *Geophysical Research Letters*, 48, e2020GL091741.

Radu, D., Berger, M., Fonteneau, R., Hardy, S., Fettweis, X., Le Du, M., Panciatici, P., Balea, L. and Ernst, D. (2019)

Complementarity assessment of South Greenland katabatic flows and West Europe wind regimes. *Energy*, 175, 393–401.

Serreze, M.C. and Francis, J.A. (2006) The Arctic on the fast track of change. *Weather*, 61, 65–69.

van As, D., Fausto, R.S., Steffen, K., Ahlstrøm, A.P., Andersen, S. B., Andersen, M.L., Box, J.E., Charalampidis, C., Citterio, M., Colgan, W.T., Edelvang, K., Larsen, S.H., Nielsen, S., Veicherts, M. and Weidick, A. (2014) Katabatic winds and piteraq storms: observations from the Greenland ice sheet. *Geologic Survey of Danemark and Greenland Bulletin*, 31, 83–86.

van den Broeke, M.R., Duynkerke, P.G. and Oerlemans, J. (1994) The observed katabatic flow at the edge of the Greenland ice sheet during GIMEX-91. *Global and Planetary Change*, 9, 3–15.

**SUPPORTING INFORMATION**

Additional supporting information can be found online in the Supporting Information section at the end of this article.